Analog simulation of stochastic systems in a metastable piecewise quasilinear potential driven by band-limited white noise

Shigeo Hayashi
Department of Applied Physics and Chemistry, University of Electro-communications, Chofugaoka, Chofu, Tokyo 182, Japan
(Received 2 May 1995)

Stochastic dynamics in a metastable potential that is linear except for finite curvatures at the bottom and barrier top has been treated using an analog simulator. Band-limited white noise is applied and the response of the system is observed as the bandwidth is increased until the noise becomes effectively white. Supplementary computer simulations have also been carried out. In the oscillation regime, i.e., for low noise intensities, the power spectrum exhibits significant deviation from that for the harmonic oscillators. Average amplitudes of the driving force have been calibrated so that peak positions of the power spectrum may produce identical results for the two simulations. The amplitude distribution has been consistent among the analog simulation, the computer simulation, and the Boltzmann distribution. For higher noise intensities, the Arrhenius plot from the analog and computer simulations has reproduced a correct barrier height, but the pre-exponential factor is about one-sixth of that obtained from Kramers's formula.

PACS number(s): 05.40.+j, 82.20.Fd

I. INTRODUCTION

From the Arrhenius law [1,2] to stochastic resonance [3], nonlinear stochastic dynamics [4] offers an alternative dimension in understanding nature. These processes can be envisaged as a barrier crossing influenced by a random force with or without another periodic force. Since only a few potentials allow us to find analytical solutions, simulation approaches [5–7] have been adopted by several investigators to solve complex problems that defy exact approaches, making it possible to assess the validity of various theories. Of these approaches, analog simulations [6,7] have a unique merit that immediate results can be obtained, although the precision may be modest compared to that of computer simulations. Furthermore, dynamics driven by colored noise or by a superposition of noise and deterministic force [8] can be investigated with little difficulty.

We have developed a type of the simulator that works in frequency space rather than in voltage space as in conventional simulators [9]. Unique features of our simulator include that the potential is piecewise quasilinear (PQL), that is, it is a metastable linear potential having finite curvatures at stationary points. The metastability is advantageous in treating escaping events if the escape is to be defined as an event in which a particle never returns the original state.

Somewhat related work dealing with metastable potential is the study of escape from metastable potentials of the polynomial form $\frac{1}{3}x^3 - \frac{1}{2}x^2$ under the influence of both exponentially correlated colored noise and sinusoidal force [10,11]. A significant difference may be expected for PQL potentials because of small curvatures at the stationary points. As a first step in the application of the simulator, however, we have applied band-limited white noise to the PQL potential in place of exponentially correlated noise, since it is a logical and immediate extension of our previous experiments on a sinusoidal driving force [12–14].

The use of band-limited white noise is another feature of our analog simulator. This noise is characterized by the spectral density s and the bandwidth B, the latter being infinite for true white noise. This is advantageous in comparing the experimental results with numerical ones, which are obtained for finite integration step size h. Since B is finite if h is finite, numerical results are actually obtained for band-limited white noise. If one can observe a phenomenon that depends on the average power but not on B, then a close comparative study is made possible. An example is the dependence of peak frequency f_{peak} of the power spectrum. If both experimental and numerical results yield an identical f_{peak}, then the two systems may be regarded as equivalent. Thus numerical calculations have also been carried out, demonstrating that the two dissimilar simulations can be unified in order to get a deeper insight into the problem in question.

Nonwhite noise of recent interest seems to be exponentially correlated noise, which tends to white noise in the limit of short correlation time [7,8]. For finite values of correlation time, however, the system obeys a generalized Langevin equation [15] and hence the system should be able to distinguish the difference from white noise, whereas band-limited white noise can "cheat" the system.

This paper is organized as follows. In Sec. II, following a brief explanation of the experimental aspects of our simulator, including band-limited white noise, a method for translating experimental escape results into physically meaningful quantities is presented. A method for straightforward numerical integration is also described. Simulation results are presented in Sec. III. More emphasis is placed on the results of analog simulation, but those of computer simulation are also included to show

that the two give consistent results provided parameters are chosen properly. Section IV concludes the paper.

II. METHOD OF ANALYSIS

A. Model

The present simulator [9] is a feedback circuit consisting of three major components: a phase detector, a loop filter (i.e., an integrator), and a voltage-controlled oscillator (VCO). The frequency x of the simulator obeys, to a good approximation, the following equation [16]:

$$\epsilon\frac{d^2x}{dt^2}+\frac{dx}{dt}+\frac{K}{\tau}V'(x)=K_0v_{\rm ext}(t), \tag{2.1}$$

where τ, currently 10 ms, is an adjustable time constant, the VCO delay time ϵ is 2.5 ms, $K=8.3\times10^5\ \mathrm{s}^{-1}$ and $K_0=2.54\times10^5\ \mathrm{Hz\,V}^{-1}$ are fixed gain parameters, and $v_{\rm ext}$ stands for external noise signal. The interaction potential $V(x)$, depicted in Fig. 1, is piecewise linear to a first-order approximation. Its form is determined by the size of a piezoelectric resonator used in the simulator and the mode of vibration (i.e., fundamental, third order, etc.) and can be well approximated by the analytical formula

$$V(x)=(f_r-x)\tan^{-1}\frac{f_r-x}{\Gamma}+(x-f_a)\tan^{-1}\frac{x-f_a}{\Gamma}-\frac{\Gamma}{2}\ln\frac{\Gamma^2+(f_r-x)^2}{\Gamma^2+(x-f_a)^2}+\frac{\pi}{2}x+\text{const}, \tag{2.2}$$

where the value of the constant is conveniently determined so that $V(f_r)=0$. This expression is derived from the phenomenological phase angle θ of the admittance [17]

$$V'(x)\equiv\theta(x)=\tan^{-1}\frac{f_r-x}{\Gamma}+\tan^{-1}\frac{x-f_a}{\Gamma}+\frac{\pi}{2}, \tag{2.3}$$

where the resonance frequency $f_r=68.1$ kHz, the antiresonance frequency $f_a=82.3$ kHz, and $\Gamma\simeq0.4$ kHz. The values of f_r and f_a are known precisely, but the accuracy of Γ is about 30%. A more exact representation for x consisting of a set of coupled differential equations has been obtained, but Eq. (2.1) suffices in reproducing essential features of the dynamics [17]. In what follows the potential well is located at f_r unless otherwise stated, but it is possible to work with the inverted potential for which the bottom is located at f_a.

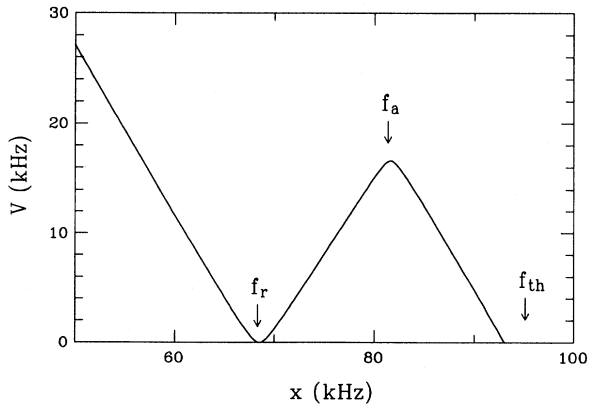

FIG. 1. Effective potential for the analog simulator. The barrier height is 18.3 kHz.

B. Band-limited white noise

The noise we use is a band-limited Gaussian noise [18], which is obtained by applying a low-pass filtering to white noise. It will be shown in Sec. III that escape dynamics is indistinguishable from that obtained with white noise, provided the bandwidth exceeds a certain characteristic bandwidth B_c. To characterize the noise, therefore, we start with the autocorrelation $R(t)$ for white noise

$$R(t)=\langle v_{\rm ext}(t)v_{\rm ext}(0)\rangle=s\delta(t), \tag{2.4}$$

where s is measured in units of $\mathrm{V^2/Hz}$. It will be shown below, however, that half of the real spectral density $\frac{1}{2}s$ is compatible with the spectral density in physical systems [see Eq. (2.23) below]. The power spectrum corresponding to Eq. (2.4) is

$$S(\omega)=\int_{-\infty}^{\infty}R(t)e^{i\omega t}dt, \tag{2.5}$$

which equals the constant s for white noise, and the inverse is

$$R(t)=\frac{1}{2\pi}\int_{-\infty}^{\infty}S(\omega)e^{-i\omega t}d\omega. \tag{2.6}$$

The average power $R(0)$ is infinite for white noise, but it is finite for the present band-limited white noise since Eq. (2.6) is reduced to

$$R(0)=2sB, \tag{2.7}$$

where the effective bandwidth B is measured in units of hertz. To calculate the power we measure the root-mean-square voltage $v_{\rm rms}$, which can be obtained as the output of an ac-to-rms converter or as the average of sampled voltages from a fast Fourier transform (FFT) power spectrum analyzer. The former data were used for the monitoring and the latter, made possible with a NF R9211A analyzer, were used for data analysis. The analyzer yields the average power in the form of $v_{\rm rms}$ defined by

$$v_{\rm rms}^2=\frac{1}{m}\sum_{i=1}^{m}v_i^2, \tag{2.8}$$

where v_i is sampled voltage and $m=800$, and Eq. (2.7) becomes

$$2sB=v_{\rm rms}^2. \tag{2.9}$$

The values of $v_{\rm rms}$ were obtained from 16 sets of waveform data.

The FFT analyzer actually yields relative values of $S(\omega)$ and therefore the proportional constant was deter-

mined by the computer so that the identity $R(0) = v_{\rm rms}^2$ held. A typical power spectrum of noise is illustrated in Fig. 2, where $s = 3.8 \times 10^{-4}$ V^2/Hz, $B = 9.2$ kHz, and $v_{\rm rms} = 2.63$ V. It also shows the cutoff characteristics of the low-pass filter.

For numerical calculations, a random force ξ is generated using the box Müller formula [19]. From a pair of random numbers η_1 and η_2 uniform in the range (0, 1), we obtain two Gaussian signals ξ_1 and ξ_2 as

$$\xi_1 = v_{\rm rms} r \cos\phi, \qquad \xi_2 = v_{\rm rms} r \sin\phi, \tag{2.10}$$

where

$$r = \sqrt{-2\ln\eta_1}, \qquad \phi = 2\pi\eta_2. \tag{2.11}$$

Numerical calculations have been confirmed to yield ξ_i's whose average really equals the preset $v_{\rm rms}$ value.

C. Scaled Langevin equations

Since the simulator works in the frequency space, we need to change dimensions in order to make a comparison with the dynamical systems of physical interest. With the replacements

$$x = x_c z, \qquad t = t_c u, \tag{2.12}$$

where z and u are dimensionless variables, Eq. (2.1) can be reduced to a scaled form

$$\frac{d^2z}{du^2} + p\frac{dz}{du} + qU'(z) = n(u), \tag{2.13}$$

where

$$p = \frac{t_c}{\epsilon}, \qquad q = \frac{t_c^2 K}{\epsilon\tau x_c} \tag{2.14}$$

and

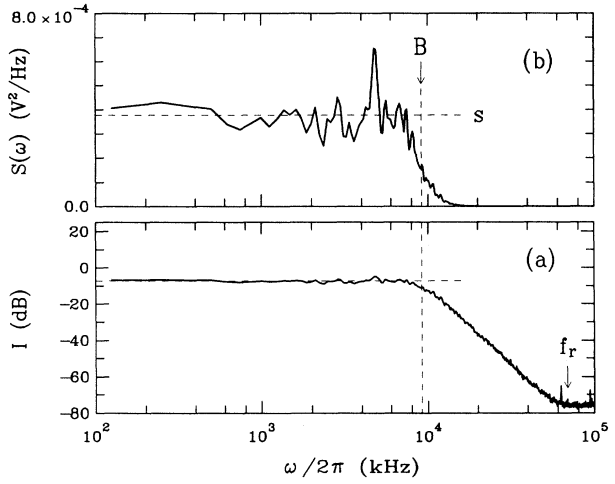

FIG. 2. Typical power spectra of noise: (a) original spectrum from the FFT analyzer, [n (dB)]= 20 $\log_{10} n$; (b) scaled spectrum.

$$\langle n(u)n(0)\rangle = rs\delta(u)\ , \tag{2.15}$$

with

$$r = \frac{1}{t_c}\left(\frac{t_c^2 K_0}{\epsilon\tau x_c}\right)^2 . \tag{2.16}$$

A similar scaled equation is also derived from the standard Langevin equation for the position of a particle:

$$m\frac{d^2y}{dt^2} + \beta\frac{dy}{dt} + W'(y) = \xi(t)\ , \tag{2.17}$$

where m is the mass, β is the friction coefficient, ξ is the random force, and the potential $W(y)$ is similar in form to that of Fig. 1 with a suitable scaling. The autocorrelation function for ξ is [15,20,21]

$$\langle\xi(t)\xi(0)\rangle = 2\beta k_B T\delta(t), \tag{2.18}$$

where k_B is the Boltzmann constant and T the absolute temperature. With the replacements

$$y = y_0 z, \qquad t = t_0 u, \tag{2.19}$$

we obtain the coefficients and autocorrelation comparable to Eqs. (2.14) and (2.15):

$$p' = \frac{\beta t_0}{m}, \qquad q' = \frac{t_0^2}{m y_0}, \tag{2.20}$$

and

$$\langle u(t)u(0)\rangle = \frac{2\beta k_B T}{t_0}\left(\frac{t_0^2}{m y_0}\right)^2 \delta(u). \tag{2.21}$$

Equating p to p' and q to q', we obtain

$$\frac{m}{\beta^2 y_0^2} W(y) = \frac{\epsilon K}{\tau x_c^2} V(x) \tag{2.22}$$

and

$$2k_B T\left(\frac{m}{\beta^2 y_0^2}\right) = \left(\frac{\epsilon K_0^2}{\tau^2 x_c^2}\right)\left(\frac{s}{\nu}\right), \tag{2.23}$$

where the potentials are defined so that their values vanish at the minimum and the extra factor ν is introduced to resolve the possible discrepancy arising from the improper definition of the spectral density; a sensible choice turns out to be $\nu = 2$. The ratio of Eq. (2.22) to Eq. (2.23) gives

$$\frac{W(y)}{k_B T} = \frac{V(x)}{\sigma}, \tag{2.24}$$

where σ, having a dimension of frequency, is defined by

$$\sigma = \frac{K_0^2}{2\tau K}\left(\frac{s}{\nu}\right) \tag{2.25}$$

and plays the role of thermal energy.

Typical values of x_c and t_c are suggested here for convenience. It seems appropriate to use the results for sinusoidal $v_{\rm ext}$, in which the system is least stable at a

frequency of $t_c^{-1} = 145$ Hz. The value of x_c may be taken as $(f_a - f_r)$, giving the barrier at $z = 1$ and the bottom at $z = 0$. Thus the suggested values are $p \simeq 2.76$, $q \simeq 18.5$, and $r \simeq 2.70 \times 10^5$ Hz/V^2. Since no unique choice of x_c and t_c is possible, the experimental values are presented without scaling.

With the simulator, we can observe the evolution of $x(t)$ or $z(u)$ from the minimum of the potential, $x = f_r$ or $z = 1$. Specifically, the simulator can register the values of λ, i.e., the lifetime for escape from the potential minimum to the location outside the potential barrier, $f_{\rm th}$ of Fig. 1. The imaginary particle never returns the potential well once it passes this point. Such a point is rather arbitrary. The values of the lifetime were measured by an on-board counter for a personal computer. For small values of λ, a modulation-domain analyzer (MDA) can also be used, since it shows directly how x evolves when it crosses the barrier. Thus the correlation between the counter outputs and the MDA wave forms has given an estimate of the counter performance: the time resolution 65 ms and the delay time 30 ms. These values set a practical lower bound to the range of λ, but a better performance would be achieved with a stand-alone counter.

D. Numerical solution of the Langevin equation

Consider the equation

$$\frac{d^2x}{dt^2} + p\frac{dx}{dt} + \theta(x) = \xi(t), \tag{2.26}$$

which is to be solved in the time interval $[t_i,\ t_{i+1}]$ $(i = 0, 1, 2, ...)$, with a fixed step size $h = t_{i+1} - t_i$. In the present paper, we approximate $V'(x) = \theta(x)$ by lines

$$\theta(x) = q_i(x - x_i) + \theta_i, \tag{2.27}$$

where

$$q_i = \theta'(x_i), \qquad x_i = x(t_i). \tag{2.28}$$

Since the equations thus derived are those for harmonic oscillators, Eq. (2.26) is solved by [21]

$$x_{i+1} = x_i + \int_0^h dt' s(t_i - t')\xi(t') + \frac{\theta(x_i)}{q_i}[1 - c(h)] + \dot{x}_i\, s(h) \tag{2.29}$$

and for its derivative

$$\dot{x}_{i+1} = \int_0^h dt' c(t_i - t')\xi(t') + \theta(x_i)s(h) + \dot{x}_i\, c(h), \tag{2.30}$$

where

$$c(t) = e^{-\frac{1}{2}pt}\cos\gamma t - \frac{1}{2}ps(t) \tag{2.31}$$

and

$$s(t) = e^{-\frac{1}{2}pt}\frac{\sin\gamma t}{\gamma t}. \tag{2.32}$$

Here γ is defined by

$$\gamma = \sqrt{q_i - \frac{1}{4}p^2}. \tag{2.33}$$

If γ is imaginary such that $\gamma = i\tilde{\gamma}$, $\cos\gamma t$ and $\sin(\gamma t)/\gamma t$ should be replaced by $\cosh\gamma t$ and $\sinh(\tilde{\gamma}u)/\tilde{\gamma}u$, respectively. The integrals can be evaluated using the trapezoidal rule by dividing h into N_h subintervals.

The numerical method here is not as efficient as standard methods [5]. For example, the method with $N_h = 2$ is half as fast as the Runge-Kutta method. In both methods the numbers of noise samples are identical. Nevertheless, we adopted the method since numerical results were used primarily for checking the experimental results.

III. RESULTS AND DISCUSSION

A. Dependence on the bandwidth of noise

Equation (2.9) suggests that the average voltage $v_{\rm rms}$ is not an essential quantity for characterizing the driving force of the dynamical system. We shall demonstrate, from analog simulation, that the spectral density s is more essential.

1. Average escape rate

With $s = 4 \times 10^{-4}$ V^2/Hz, 1000 samples of the lifetime have been registered for various values of B. Reciprocals of the average of λ, i.e., k' defined by Eq. (3.10) below, are shown in Fig. 3(a). k' increases with the frequency in the low-frequency region and, after an overshoot, levels off to a plateau value, which can be regarded as the rate for the true white noise. If the characteristic frequency may be defined as the frequency at which the value in question is half the plateau value, as is consistent with the cutoff frequency of Fig. 2, then we have

$$B_{c1} \sim 200 \text{ Hz}.$$

This noise-induced escape may be related to escape caused by sinusoidal force. Thus, for purposes of comparison, the critical amplitude a_c for escaping under the influence of the following sine waves is plotted in Fig. 3(b) as a function of the frequency $f_{\rm sine}$:

$$v_{\rm ext}(t) = a\sin(2\pi f_{\rm sine}t). \tag{3.1}$$

The escape behavior varies, depending on whether Eq. (3.1) is applied from $t = 0$ or a is increased as slowly as possible from a sufficiently small value, but the characteristic frequency f_{c1} of 145 Hz, for which the system is the least stable is the same in either mode. The graph rises steeply at another characteristic frequency f_{c2} of 200 Hz, for which barrier recrossing was observed [14]. B_{c1}, the lowest of the characteristic bandwidths observed in the present paper, is of the same magnitude as f_{c1} and f_{c2}.

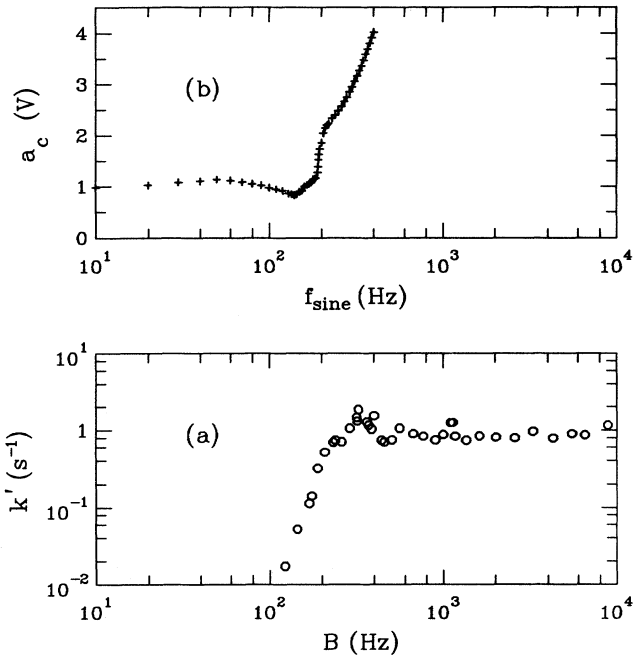

FIG. 3. (a) Dependence of the average escape rate on the bandwidth of noise. (b) Critical amplitude for the sinusoidal driving force.

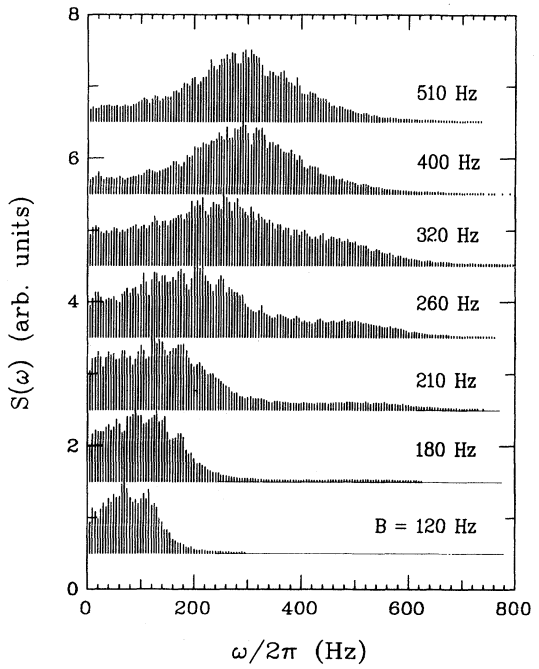

FIG. 4. Power spectra of x for various bandwidths B of noise.

the present paper, is of the same magnitude as f_{c1} and f_{c2}.

2. *Most probable frequency of nonlinear oscillation and width of amplitude distribution*

If the spectral density is reduced so that the escape event can almost never occur, then the simulator system can be looked upon as a nonlinear oscillator. The oscillation can be characterized by the power spectrum $S(\omega)$ and the amplitude distribution about the average $\rho(\Delta x)$, both of which can be made possible with the MDA. The power spectrum can be calculated conveniently as the squared moduli of FFT's for about 2000 samples of $x(t)$ multiplied by Hanning's window function [22].

For a spectral density of $s = 1 \times 10^{-4}$ V^2/Hz, the power spectra are depicted in Fig. 4 for several values of the bandwidth B. They have a peak at $\omega/2\pi = f_{\text{peak}}$. A peculiar feature is that still another peak is seen around $\omega/2\pi \sim 500$ Hz in the range $B = 210-260$ Hz. This peak should be a genuine one since it was also observed for the inverted potential with the bottom at f_a. In other words, four peaks appear in the extended ω range $(-\infty, +\infty)$. This is in contrast to the harminic oscillator driven by colored noise, for which at most three peaks can be obsereved [23].

The dependence of f_{peak} on the bandwidth is shown in Fig. 5(a). It has a characteristic frequency

$$B_{c2} \sim 220 \text{ Hz}.$$

Still another quantity characterizing nonlinear oscillator is the width of distribution $\rho(x - f_a)$, which can be observed directly on the MDA. The results are shown in Fig. 5(b), where a characteristic frequency is

$$B_{c3} \sim 500 \text{ Hz}.$$

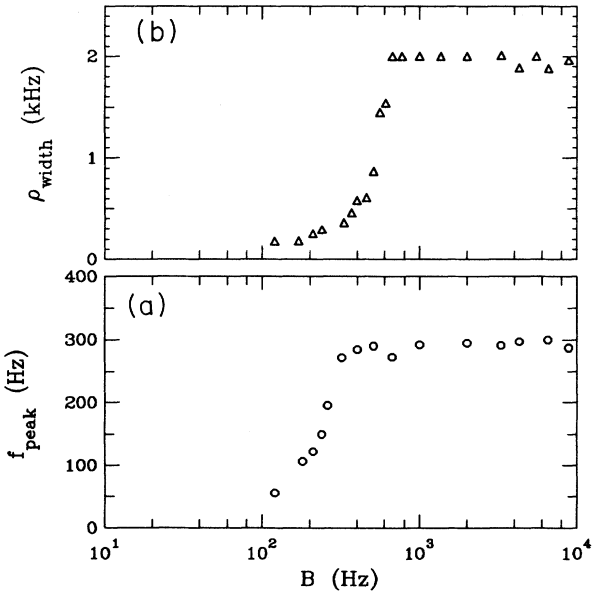

FIG. 5. Dependence on the bandwidth of the noise in the weak noise regime. (a) Peak frequency of the power spectrum. (b) Width of the amplitude distribution.

A similar B_{c3} value was obtained for $\rho(x - f_r)$, but this distribution was not preferable because of the shape being distorted probably due to an imperfection of the simulator. From these results on the B_c's, it is seen that the dynamical system experiences the noise as if it were white when $B \gg B_c \equiv \max\{B_{c1}, B_{c2}, B_{c3}\}$ and that the characteristic frequencies increase as the noise power is decreased. The bandwidth dependence may be observed for other phenomena, but it seems unlikely that the magnitude of B_c will increase significantly from the present value.

B. Dependence of the power spectrum on noise power

As has been demonstrated in Sec. III A, the spectral shape is unaffected by changing the bandwidth B, provided B exceeds some characteristic frequency B_c. What if the spectral density s is varied while the bandwidth B is fixed? It has been found that the dependence on the amplitude $v_{\rm rms}$ is more tractable than the dependence on $s \propto v_{\rm rms}$ since the relationship is close to linear. Figure 6 shows how the power spectra change as $v_{\rm rms}$ is increased while B is fixed at 9.2 kHz, which is greater than B_c. Peaks of the spectra shift to lower frequencies with increasing $v_{\rm rms}$. This behavior should be peculiar to PQL potentials since $f_{\rm peak}$ is not affected by noise power in the case of harmonic potentials driven by white noise [24] or exponentially correlated noise [23].

The relationship between $f_{\rm peak}$ and $v_{\rm rms}$ is summarized in Fig. 7, where numerical results are also included. The numerical calculation has been carried out for an integration step width of 0.02 ms, a sampling interval of 0.08 ms, and the number of trapezoidal steps $N_h = 2$, thus incorporating two noise inputs within each integration step.

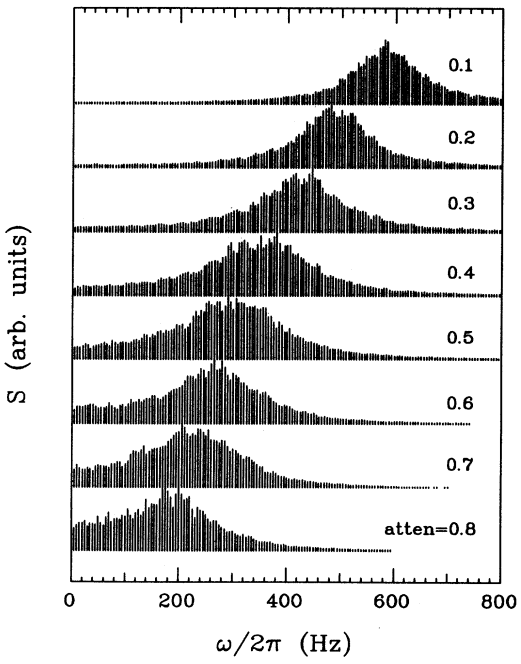

FIG. 6. Power spectra of x for various values of the spectral density s of noise. s =(attenuation)$^2 \times 4.0 \times 10^{-4}$ V^2 Hz^{-1}.

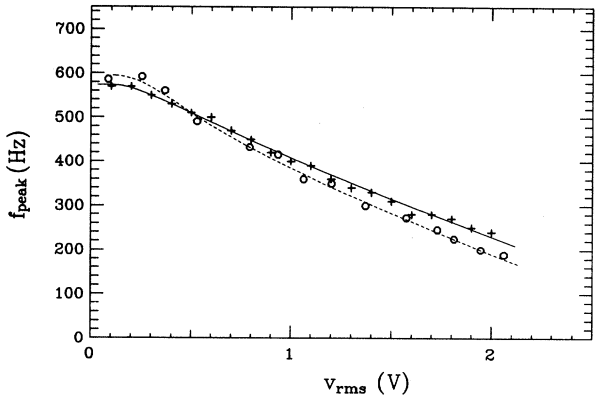

FIG. 7. Dependence of the peak frequency on the noise power. Circles, analog simulation; crosses, computer simulation.

We can use Fig. 7 for calibrating $v_{\rm rms}$'s for analog and numerical simulations $v_{\rm rms,ana}$ and $v_{\rm rms,num}$, although no calibration would be required if the value of B were somewhat higher. Since the two curves should converge on the same value as $v_{\rm rms} \to 0$, as discussed in the following paragraph, we compare the slopes and obtain the calibration relationship

$$v_{\rm rms,ana} = \kappa(B) v_{\rm rms,num}, \tag{3.2}$$

with $\kappa(9.2\ \text{kHz}) \approx 0.96$. Note that the conversion factor κ depends on the bandwidth.

In the limit $v_{\rm rms} \to 0$, $f_{\rm peak}$ converges on a finite value $f_{\rm hrm}$ corresponding to small-amplitude oscillation at the bottom of the harmonic potential, for which a power-series expansion of Eq. (2.2) gives

$$V'(x) \cong \frac{1}{\Gamma}(x - f_r). \tag{3.3}$$

Inserting Eq. (3.3) into Eq. (2.1) yields an equation that is the same as Eqs. (2.26) and (2.33) with $\theta_i = 0$, $x_i = 0$, $p = [0.4 \times 10^3\ (\text{Hz})]t_c$, and

$$q_i = \frac{t_c^2 K}{\epsilon\tau\Gamma} \simeq [4.2 \times 10^3\ (\text{Hz})^2]t_c^2. \tag{3.4}$$

The squared modulus of the Fourier transform of Eq. (2.29) is a practical estimation of the power spectrum [24]

$$S(\omega) = s_\xi \left[(\omega - \gamma)^2 + \left(\frac{p}{2}\right)^2\right]^{-1} \left[(\omega + \gamma)^2 + \left(\frac{p}{2}\right)^2\right]^{-1}, \tag{3.5}$$

where s_ξ is the spectral density for $\xi(t)$. The frequency in the low-power limit is thus given by the peak frequency of Eq. (3.5)

$$f_{\text{peak}} \to f_{\text{hrm}} \simeq \frac{\gamma}{2\pi t_c} \simeq \frac{1}{2\pi}\left(\frac{K}{\epsilon\tau\Gamma}\right)^{\frac{1}{2}} \simeq 580 \text{ Hz}, \quad (3.6)$$

which is in good agreement with the experiment, as seen from Fig. 7. The value of f_{peak} would not be affected by the spectral density of noise if Eq. (3.5) were valid for all values of s_ξ, and thus Fig. 7 shows a power nonlinearity in piecewise linear potentials.

C. Amplitude distribution for the nonlinear oscillator

A typical example of $\rho(x)$ is shown in Fig. 8, where $s = 9.1 \times 10^{-5}$ V^2/Hz, $B = 9.2$ kHz, and $v_{\text{rms}} = v_{\text{rms,ana}} = 1.27$ V. Here the distribution about f_a is shown since that about f_r is distorted probably because of a low impedance of the piezoelectric resonator at f_r. Relative peak heights are the only parameters that can be adjusted. The experimental results are in good agreement with the numerical results calculated for $v_{\text{rms,num}} = v_{\text{rms,ana}}/\kappa(9.2 \text{ kHz})$.

The figure also shows an analytical result corresponding to the Boltzmann distribution

$$\rho(x) = \text{const} \times \exp\left[-\frac{V(x)}{\sigma}\right], \quad (3.7)$$

which can be derived from the correspondence, Eq. (2.24), between the dynamics in the experimental phase space $(x, \dot{x})$ and that in the physical phase space $(y, \dot{y})$. An alternative derivation is to consider the random walk that obeys Eq. (2.17) [25]. Here the value of σ is evaluated for $\frac{1}{2}s$ using Eq. (2.25), where $v_{\text{rms,ana}}$ is adopted for v_{rms}. If the value of σ were reduced by 20%, then perfect agreement with both of experimental and numerical data would be achieved, but it seems appropriate to regard the discrepancy as representing the inaccuracy of our analog simulator. The consistency among three sets of data validates the choice of $\nu = 2$ for σ defined by Eq. (2.25). In passing, we note that no correction would have been required if we had adopted $4\beta k_B T$ for the density [24] in Eq. (2.18).

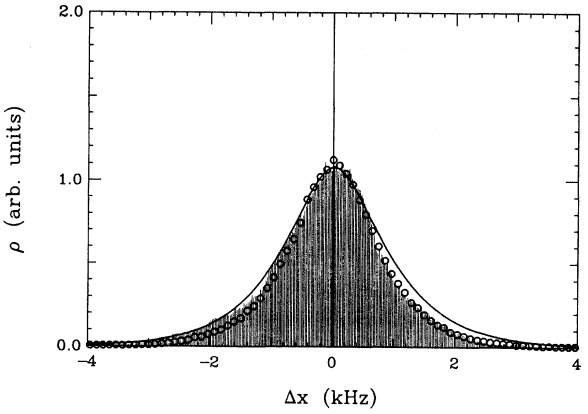

FIG. 8. Distribution of $x(t)$. Shaded region, analog simulation; circles, computer simulation; line, Boltzmann distribution.

D. Dependence of the escape rate on noise power

1. Distribution of the lifetime

Let us turn to the escape phenomena taking place for the increased spectral density of noise. The behavior can be characterized by an escape rate constant k, which may be defined by the relationship

$$\frac{dN}{dt} = -kN, \quad (3.8)$$

where N is the number of imaginary particles in the potential well. Integrating Eq. (3.8) leads to the time dependence of the probability $P_{\text{obs}}(t)$ for observing a particle at time t,

$$P_{\text{obs}}(t) = P_{\text{obs}}(0)\exp(-kt).$$

Let $P_\lambda d\lambda$ be probability that the lifetime is within the range between λ and $\lambda + d\lambda$. Then it must be possible to identify P_{obs} as P_λ. The distribution P_λ can only be inferred from sampling. A histogram of the distribution for the noise data of Fig. 2 is shown in Fig. 9 for 1000 samples. The distribution is well represented by

$$P_\lambda \propto \exp(-k\lambda) \quad (3.9)$$

and therefore a least-squares fit yields the desired rate constant. A more practicable estimate of k is to calculate the reciprocal average of the lifetime

$$k' = \frac{\sum P_\lambda}{\sum \lambda P_\lambda}, \quad (3.10)$$

which will be equal to k if Eq. (3.9) holds.

2. Arrhenius plot

Equation (2.24) suggests that Arrhenius law holds as in the physical world where the law is manifested by

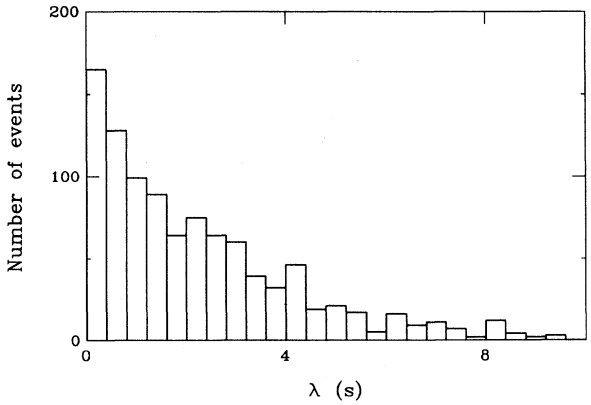

FIG. 9. Typical histogram for the distribution of the lifetime λ.

$$k_{\rm phys} = A_{\rm phys} \exp\left(-\frac{E_{\rm act}}{k_B T}\right), \tag{3.11}$$

where $E_{\rm act}$ is the activation energy. In the analog simulation, the Arrhenius law should be expressed by

$$k_{\rm ana} = A_{\rm ana} \exp\left(-\frac{\Delta V}{\sigma}\right), \tag{3.12}$$

where ΔV is the equivalent barrier height in frequency. The exact value of ΔV, 18.3 kHz, is readily seen from Fig. 1.

The plot of $\log_{10} k_{\rm ana}$ against σ^{-1} is shown in Fig. 10, where the number of samples is 1000 for analog simulation and 500 for computer simulation. Statistical errors are approximately of the same order of magnitude as the size of the symbols. The plot is linear in conformity with the Arrhenius law, giving the parameters

$$A_{\rm ana} = 93 \text{ Hz}, \qquad \Delta V = 18.4 \text{ kHz}.$$

Since the correct barrier height is reproduced, the choice of $\nu = 2$ is found be legitimate in Eq. (2.25). The consistency between the rate constants from analog and computer simulations confirms the choice of κ. These points have also been noted in Sec. III C.

The pre-exponential factor may be compared with the Kramers formula [1,26]

$$A_{\rm Kramers} = f_{\rm hrm}\left[\sqrt{1+(4\pi\epsilon f^{\ddagger}_{\rm hrm})^{-2}} - (4\pi\epsilon f^{\ddagger}_{\rm hrm})^{-1}\right], \tag{3.13}$$

where the imaginary frequency $if^{\ddagger}_{\rm hrm}$ represents the passage over the barrier and the square brackets represent correction to the transition-state theory. Numerically we have $f^{\ddagger}_{\rm hrm} = f_{\rm hrm}$, as seen from Fig. 1. Since we have $(4\pi\epsilon f^{\ddagger}_{\rm hrm})^{-1} \simeq 0.1$, Eq. (3.13) leads to $A_{\rm Kramers} \simeq f_{\rm hrm} = 580$ Hz, which is about six times higher than $A_{\rm ana}$. The disagreement is not surprising since the Kramers formula is based on a power-series expansion of the potential at stationary points of the potential. It seems likely that the pre-exponential factor is somehow related to the characteristic frequencies f_{c1} and f_{c2} of the sinusoidal driving force discussed in Sec. III A 1.

The complementary nature of the analog and computer simulations is exemplified in Fig. 10; if the excape rate is high, the analog simulation tends to yield poor results due to finite time resolution, while millions of random numbers need to be generated for the low escape rates.

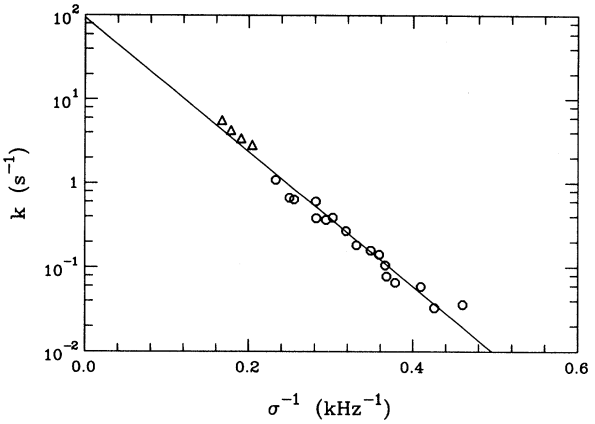

FIG. 10. Arrhenius plot of the escape rate k vs the effective temperature σ. Circles, analog simulation; triangles, computer simulation.

IV. CONCLUSION

We have presented some experimental results, analog and numerical, for a piecewise quasilinear potential. A comparison with theory in the low-power regime has yielded a correct relationship between the spectral density for the physical system and that for the simulator. This has been made possible owing to the finite bandwidth of noise. The finiteness has resulted in the emergence of an extra peak in the power spectrum and the appearance of characteristic bandwidths B_{c1}, B_{c2}, and B_{c3}. The lowest of these is close to the escape due to the sinusoidal driving force and the highest of these to the harmonic limit. The dependence of the escape rate on the noise power conforms with the Arrhenius law, but the pre-exponential factor is considerably smaller than that predicted by the transition-state theory, necessitating an improved theory.

[1] H. A. Kramers, Physica **7**, 284 (1940).
[2] P. Hänggi, P. Talkner, and M. Berkovec, Rev. Mod. Phys. **62**, 251 (1990).
[3] See, for example, T. Kapitaniak, Phys. Rev. E **49**, 5855 (1994), and references therein.
[4] *Noise in Nonlinear Dynamical Systems*, edited by F. Moss and P.V.E. McClintock (Cambridge University Press, Cambridge, 1989), Vols. 1–3.
[5] R. Mannella, Ref. [4], Vol. 3, p. 189.
[6] L. Fronzoni, Ref. [4], Vol. 3, p. 222.
[7] P. V. E. McClintock and F. Moss, Ref. [4], Vol. 3, p. 243.
[8] F. Marchesoni, E. Manichella-Saetta, M. Pochini, and S. Santucci, Phys. Rev. A **15**, 3058 (1988); L. Gammaitoni, F. Marchesoni, E. Manichella-Saetta, and S. Santucci, Phys. Rev. Lett. **62**, 349 (1989).
[9] S. Hayashi, Rev. Sci. Instrum. **64**, 3258 (1993).
[10] I. Dayan, M. Gittermann, and G. H. Weiss, Phys. Rev. A **46**, 757 (1992); M. Gittermann and G. H. Weiss, J. Stat. Phys. **70**, 107 (1993).
[11] J. M. Casado and M. Morillo, Phys. Rev. E **49**, 1136 (1994).
[12] S. Hayashi, Jpn. J. Appl. Phys. **32**, 2314 (1993).
[13] S. Hayashi, Jpn. J. Appl. Phys. **33**, 3121 (1994).
[14] S. Hayashi, Jpn. J. Appl. Phys. **34**, 2502 (1995).

[15] R. Kubo, Rep. Prog. Phys. **29**, 255 (1966).
[16] S. Hayashi, IEEE Trans. **UFFC-38**, 231 (1991).
[17] S. Hayashi, IEEE Trans. **UFFC-39**, 787 (1992).
[18] M. Schwartz, *Information Transmission, Modulation, and Noise* (McGraw-Hill, New York, 1959), p. 404.
[19] W. H. Press, B. P. Flannery, S. A. Teukolsky, and W. T. Vetterling, *Numerical Recipes* (Cambridge University Press, Cambridge, 1986).
[20] A. Papoulis, *Probability, Random Variables, and Stochastic Processes* (McGraw-Hill, New York, 1965).
[21] S. Chandrasekhar, Rev. Mod. Phys. **15**, 1 (1943).
[22] E. O. Brigham, *Fast Fourier Transform* (Prentice-Hall, Englewood Cliffs, NJ, 1974).
[23] J. Masoliver and J. M. Porrà, Phys. Rev. E **48**, 4309 (1993).
[24] M. C. Wang and G. E. Uhlenbeck, Rev. Mod. Phys. **17**, 323 (1945).
[25] M. Kac, Am. Math. Mon. **54**, (7): 369 (1947).
[26] J. I. Steinfeld, J. S. Francisco, and W. L. Hase, *Chemical Kinetics and Dynamics* (Prentice-Hall, Englewood Cliffs, NJ, 1989).